Research Article

Deep Learning Approaches for Ground Penetrating Radar Detection for Archaeological Applications

Rebecca Koleth

Phillips Academy Andover, 7 Chapel Ave, Andover, MA 01810, United States

ABSTRACT

Ground Penetrating Radar (GPR) is an essential non-invasive method in archaeology for finding archaeological features below the surface. However, interpreting the data can be difficult due to its complexity and noise. This research investigates the application of deep learning models to enhance the detection and interpretation of subsurface archaeological features using GPR data. Due to the scarcity of publicly available annotated GPR datasets, simulated data generated using the gprMax software is utilized. A Convolutional Neural Network (CNN) is built with TensorFlow and Keras. It focuses on creating bounding boxes around hyperbolic reflection signatures in B-scan radargrams. These simulations feature a buried perfect electric conductor (PEC) cylinder in a dielectric half-space. The model showed promising results, with Intersection over Union (IoU) scores of 0.93 reflecting accurate localization on test samples. This study establishes the foundation for future applications of deep learning to archaeological GPR data analysis. It also demonstrates that simulation-based training can be effective and provides a basic model where annotated samples are often scarce. This contribution is important because it positions simulation-driven training as a cost-effective option for archaeological geophysics. Data shortages have often limited the use of AI in this field. By presenting a CNN framework that adapts well to new simulated conditions, the study emphasizes the future potential of hybrid methods that combine synthetic and real data.

Keywords: Ground Penetrating Radar; Convolutional Neural Networks; Archaeology; Data Interpretation; gprMax, TensorFlow

INTRODUCTION

Ground Penetrating Radar is a widely used, non-invasive geophysical method in archaeology, employed to detect subsurface features without excavation (1). It has changed archaeological prospection by allowing the non-destructive mapping of subsurface features, such as buried structures, graves, and artifacts (2). In the case of concrete bridges, GPR served as a practical tool for inspecting the structural durability of the concrete. The GPR method facilitated faster data acquisition and reduced traffic interference by recording data from the underside of the bridge deck (3). GPR works by sending electromagnetic waves into the ground and recording reflections from differences in materials (4). Data collected from archaeological surveys consists of two-dimensional reflection profiles called B-scans (5). These B-scans often show specific hyperbolic patterns that indicate buried objects (6). However, interpreting

Corresponding author: Rebecca Koleth, E-mail: rebeccakoleth@gmail.com.

Accepted September 29, 2025
https://doi.org/10.70251/HYJR2348.35549555

GPR data is complicated. It can be affected by factors like signal loss, changes in the environment, and clutter from mixed soils. As a result, interpreting GPR data is challenging due to its noisy, complex nature and the variability of subsurface environments (7). Traditionally, this interpretation relies heavily on expert manual analysis (2), which is time-consuming, subject to human error, and can lead to inconsistencies.

Recent advances in deep learning, particularly Convolutional Neural Networks, provide opportunities to automate and enhance the detection and classification of archaeological features in GPR data (8, 9). Despite promising results in various studies, the limited availability of large, annotated archaeological GPR datasets remains a significant challenge (10). Real-world archaeological surveys produce diverse, site-specific data, and labeling this data requires expert knowledge (11), which limits the available training data.

This research addresses this gap by simulating GPR B-scan data with known buried objects using gprMax and developing CNN models to detect and localize these features (12). By simulating controlled scenarios like a buried metal cylinder, I create annotated B-scans that imitate archaeological features. A CNN is trained to locate these features through bounding box regression, demonstrating proof of concept. This simulation-based method establishes a transferable model, and similar techniques can be used for archaeological GPR by fine-tuning with limited real data (13). This simulation-driven strategy offers two main benefits. First, it produces a large amount of consistent, labeled data without needing costly field campaigns. Second, it enables the systematic variation of subsurface parameters to test CNN performance under controlled conditions.

METHODS

Data Simulation

Due to the limited availability of public, annotated archaeological GPR datasets, synthetic data was generated using the gprMax simulation software (14, 15). Each simulation modeled a perfect electric conductor (PEC) cylinder buried in a dielectric half-space, producing B-scan radargrams representing the subsurface reflections, approximating archaeological scenarios like metallic artifacts or voids (16). The transmitting antenna was a z-polarized Hertzian dipole driven by a 1.5 GHz Ricker wavelet. A co-moving receiver was positioned in a common-offset configuration relative to the transmitter. The computational domain used uniform grid discretization and a fixed simulation time window. The simulation domain was 0.120 m × 0.210 m × 0.002 m with spatial discretization of 0.002 m in all directions (Figure 1) and a time window of 3 ns. The half-space material had a relative permittivity of 6, conductivity of 0 S/m, relative permeability of 1, and magnetic loss of 0. The transmitter and receiver were stepped laterally in equal increments to produce a sequence of A-scans, which were stacked to form each B-scan radargram.

These simulation parameters were configured to approximate realistic GPR survey conditions. These simulated datasets provided the input images for training and evaluating the CNN models. From each gprMax output, the Ez field component was extracted and normalized to ensure consistent amplitude scaling. The raw GPR signals were then reshaped into single-channel tensors for compatibility with convolutional neural networks. Ground-truth bounding boxes enclosing the buried cylinder's hyperbolic reflection signature were analytically derived from the known object location, survey geometry, and wave propagation velocity, using the calculated hyperbola apex and fixed offsets in trace and time indices. These coordinates were normalized to the radargram dimensions, yielding scale-invariant labels for supervised learning.

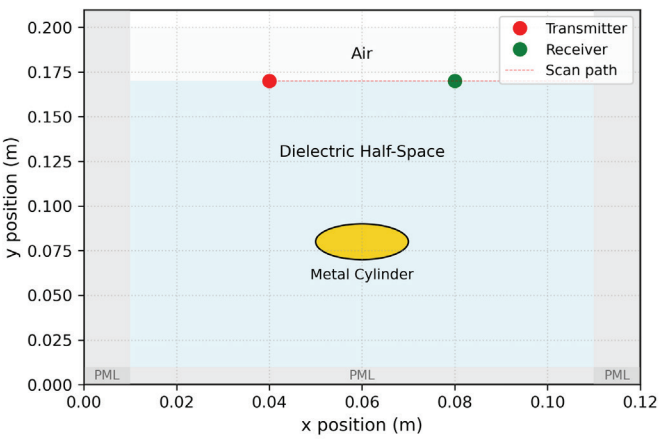

Figure 1. Simulation setup in gprMax. A PEC cylinder buried in a dielectric half-space. The transmitter (Tx) and receiver (Rx) are shown in a common-offset configuration, scanning laterally to produce the B-scan. This controlled scenario generates hyperbolic reflections that mimic buried archaeological objects such as metallic artifacts or voids.

Convolutional Neural Network Architecture

A Convolutional Neural Network was implemented using the TensorFlow and Keras frameworks to perform object localization on simulated B-scan radargrams. The model architecture consisted of three convolutional layers with ReLU activations, interleaved with max-pooling layers to progressively extract spatial features and reduce dimensionality. The first convolutional layer used 32 filters with a 5 × 5 kernel, followed by a second and third convolutional layer using 64 filters with 3 × 3 kernels. Max-pooling layers with 2 × 2 windows followed the first two convolutional layers. After the convolutional feature extraction blocks, the resulting feature maps were flattened and passed through a fully connected dense layer of 128 ReLU-activated units. A dropout layer with a dropout rate of 0.2 was included to reduce overfitting. Following this, the network regressed the bounding box coordinates of the detected subsurface object, yielding four normalized values that define the object's position within the radargram. Input radargrams were preprocessed by scaling their amplitude values to the [0,1] range using min-max normalization (17). The data were reshaped into 3D tensors of shape (time steps, traces, 1), representing grayscale images suitable for CNN input. The model was trained using the Mean Squared Error (MSE) loss function, optimized with the Adam optimizer using a learning rate of 0.001 and over 100 epochs with a batch size of 4. A validation split of 20% was used, and TensorBoard was employed to monitor training and validation loss in real time (18). Training was performed on the simulated dataset with data augmentation applied to improve model robustness, including geometric transformations and noise injection (17). Model performance was monitored through validation loss, and early stopping was used to prevent overfitting.

The CNN architecture for this study was designed as a custom, lightweight network rather than adopting more complex established models like Faster R-CNN or U-Net. This decision was motivated by several factors specific to the scope and goals of this work. While architectures such as Faster R-CNN are powerful for object detection in natural images, they involve region proposal networks and two-stage detection processes that are computationally intensive and often require very large datasets for training. Similarly, U-Net is a leading architecture for semantic segmentation, but was excessive for the task of single-object localisation in this proof-of-concept study. Given the controlled nature of the simulated data (featuring a single hyperbolic target) and the objective of developing a computationally efficient model suitable for potential future deployment on portable field hardware, a simpler, custom CNN was deemed optimal. This architecture is sufficiently complex to learn the distinctive hyperbolic features from B-scans but remains lightweight, reducing the risk of overfitting on the limited simulation dataset and enabling faster training and inference.

The choice of a lightweight CNN, with three convolutional layers and modest parameter counts, is also to balance between detection accuracy and computational efficiency (19). This design makes the model suitable for use in portable archaeological field equipment, where computing resources are limited (Figure 2).

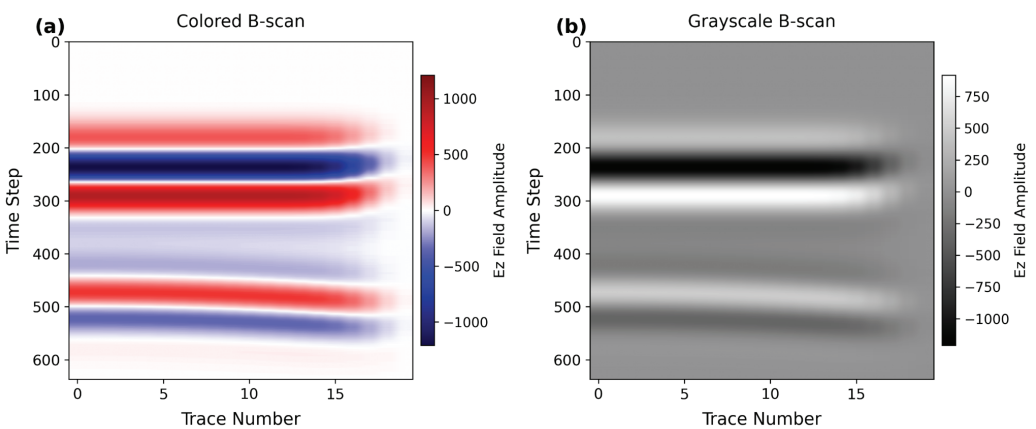

Figure 2. A B-scan image of a metallic cylinder embedded in a uniform dielectric half-space in color and grayscale. The B-scan radargram shows the normalized Ez field. The prominent hyperbola represents the reflection from the buried cylinder in Figure 1, with background noise included to simulate realistic survey conditions.

RESULTS

The trained CNN successfully identified and localized the buried cylinder within simulated GPR B-scan data. Visual inspection of predictions showed close alignment between the predicted bounding boxes and the true object locations. Quantitative evaluation using mean squared error loss indicated effective convergence during training, with validation results confirming the model's generalization on unseen simulated samples. These initial results demonstrate the feasibility of using CNNs for automated GPR feature detection and provide a foundation for extending the approach to real archaeological datasets (Figure 3).

In addition to qualitative inspection, the reliability of the CNN is shown by stable convergence behavior. The training and validation loss curves show minimal overfitting. The IoU, calculated as the overlap between the predicted and true boxes divided by their union, is around 0.93, indicating high accuracy (20). Training converged with a final validation MSE of 0.002, reflecting a minimal prediction error (Figure 4), which demonstrates the accuracy of the bounding box regression (21). These outcomes validate the model's ability to detect hyperbolic signatures, with IoU suggesting potential for archaeological applications (Figures 5 and 6).

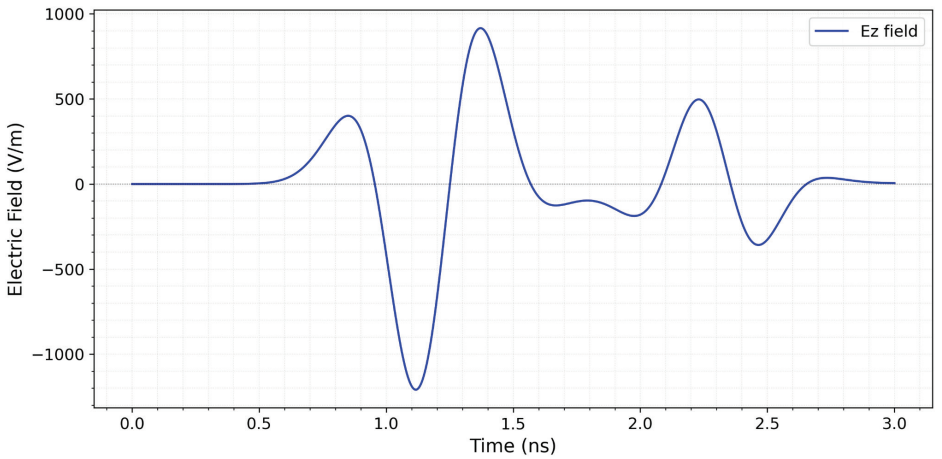

Figure 3. Representation A-scan (single trace) extracted from the simulated metal cylinder. This plot shows the raw reflected signal at a single lateral position, illustrating how individual traces contribute to the construction of the B-scan radargram.

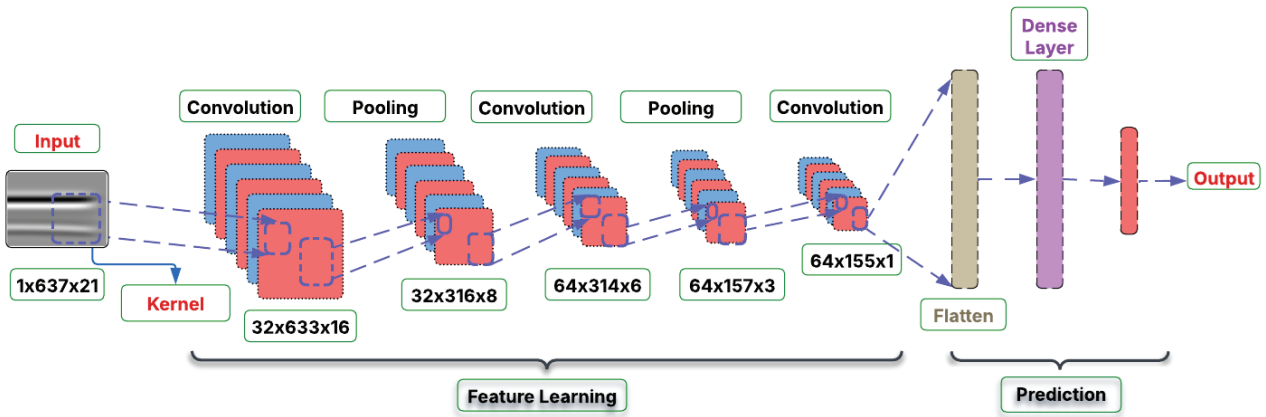

Figure 4. Architecture of the CNN model. The figure illustrates the three convolutional layers, max pooling layers, dense fully connected layer, and final regression output. The inclusion of dropout regularization and the compact depth of the architecture are designed to balance accuracy with computational efficiency.

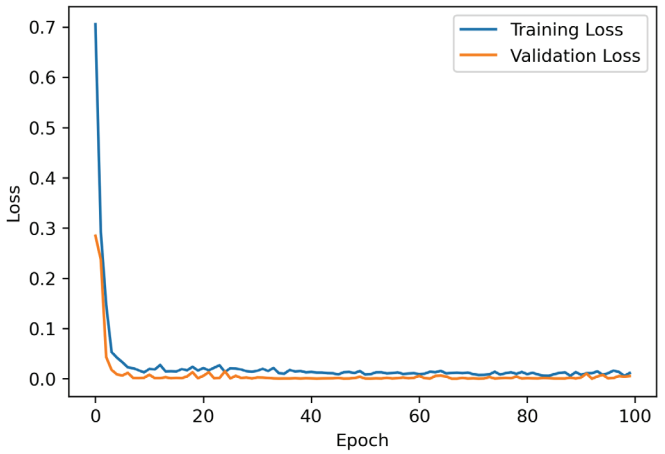

Figure 5. Training and validation loss curves for 100 epochs. Both curves converge smoothly with no significant divergence, demonstrating that the CNN generalizes well without overfitting, partly due to dropout and data augmentation.

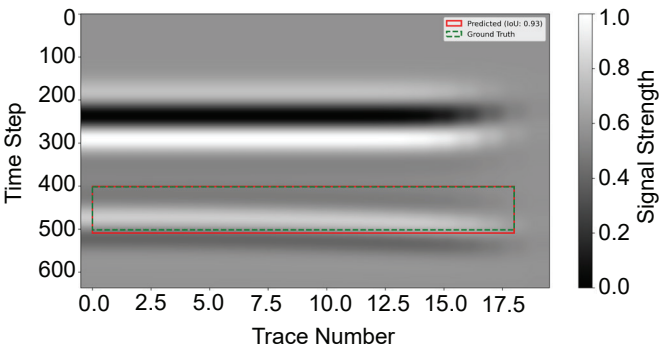

Figure 6. Comparison of predicted (red solid) and ground-truth (green-dashed) bounding boxes on a sample B-scan. IoU = 0.93, showing precise localization of the buried object and strong agreement with ground-truth annotations.

DISCUSSION

The results highlight the ability of CNNs to automate GPR interpretation. The model demonstrated quite accurate localization in simulated data. The high IoU scores confirm that the architecture effectively captures spatial hierarchies, from edges to full hyperbolas, even with a modest dataset. However, simulations simplify conditions. In reality, archaeological GPR faces varying soils, multiple objects, and artifacts (22).

A major contribution is addressing the lack of data in archaeological GPR. Annotated field datasets are rare because of excavation costs, sensitivity of sites, and the need for expert labeling (15, 23). My simulation-driven method provides a new strategy. gprMax can model site-specific features, such as walls and graves, to create labeled data for training (24). This can be fine-tuned on a few real samples using transfer learning (25). This approach could make AI applications more accessible in archaeology, lessening the need for large datasets.

Beyond the immediate contributions, the study highlights how CNNs can transform archaeological prospection workflows. By reducing the need for expert manual interpretation, automated detection can speed up survey analysis and boost reproducibility (26). Compared to traditional methods, the CNN significantly decreases interpretation time, indicating real benefits for large-scale surveys (27). Furthermore, the strong IoU score in a simulated environment shows that CNNs can pave the way for real-time field applications, especially when combined with portable hardware accelerators.

Nevertheless, limitations remain. CNNs are naturally data-hungry, and their reliance on simulation risks overfitting to synthetic artifacts (28). Addressing the domain gap between simulated and real-world radargrams will require improved strategies such as domain adaptation, adversarial learning, or physics-informed neural networks. Moreover, archaeological targets are often complex, such as intersecting structures and diverse soils (29, 30). This complexity means that the single-object detection method needs to change to multi-object segmentation approaches to be ready for field use (31). Therefore, the main limitations include the assumption of single objects and the gap between simulations and reality. Future work should focus on integrating multi-object detection and domain adaptation techniques (32). This includes a variety of simulations with different depths and materials, along with real data combinations, and could boost generalizability.

CONCLUSION

This study improves GPR analysis for archaeology by creating a CNN for locating objects with simulated data. It addresses the challenges posed by limited annotated datasets. The model's accuracy shows that simulation can be effectively used to train a model and adapted to real datasets. By promoting automated object interpretation, this work aids in efficient prospection.

This work offers three main contributions: first, the design of a lightweight CNN architecture that competes well with existing methods; second, the demonstration that simulation-based training can address the lack of annotated archaeological GPR datasets; and third, the creation of a framework that can be adjusted with limited real data for practical use.

For the future, it will be important to expand the dataset to include multi-object simulations and to test the model on archaeological field data. Integrating CNN-based interpretation into real-time survey tools could change archeological prospection, making non-invasive investigations more efficient and organized. This work provides not just a proof of concept but also a guide for future archaeological geophysics driven by deep learning.

ACKNOWLEDGMENTS

I sincerely thank everyone who helped me with this project. This includes mentors, colleagues, and peers who offered guidance, encouragement, and support throughout the research. Their feedback and suggestions greatly improved the quality of this work. I also thank the anonymous reviewer for their constructive feedback, which greatly improved the manuscript.

DATA AVAILABILITY

The deep learning models in this study are implemented using publicly available Python packages, including TensorFlow and Keras. The input parameters for the data generation as well as the code used for training and evaluation, are openly available on Zenodo at https://doi.org/10.5281/zenodo.16934316.

CONFLICT OF INTERESTS

The author declares that there is no conflict of interest regarding the publication of this paper.

REFERENCES

1. Solla M, Lorenzo H, Novo A, Riveiro B. Evaluation of ancient structures by GPR (ground penetrating radar): The arch bridges of Galicia (Spain).
2. Manataki M, Vafidis A, Sarris A. GPR Data Interpretation Approaches in Archaeological Prospection. *Appl Sci*. 2021 Aug 17; 11 (16): 7531. https://doi.org/10.3390/app11167531
3. Hugenschmidt J, Mastrangelo R. GPR inspection of concrete bridges. *Cem Concr Compos.* 2006 Apr; 28 (4): 384-92. https://doi.org/10.1016/j.cemconcomp.2006.02.016
4. Küçükdemirci M, Sarris A. Deep learning based automated analysis of archaeo-geophysical images. *Archaeol Prospect*. 2020 Apr; 27 (2): 107-18. https://doi.org/10.1002/arp.1763
5. Küçükdemirci M, Sarris A. GPR Data Processing and Interpretation Based on Artificial Intelligence Approaches: Future Perspectives for Archaeological Prospection. *Remote Sens.* 2022 July 13; 14 (14): 3377. https://doi.org/10.3390/rs14143377
6. Bonsall J, editor. New Global Perspectives on Archaeological Prospection: 13th International Conference on Archaeological Prospection, 28 August - 1 September 2019, Sligo - Ireland [Internet]. Archaeopress Publishing Ltd; 2019 [accessed 2025-08-19]. Available from: http://www.jstor.org/stable/10.2307/jj.15135979. https://doi.org/10.2307/jj.15135979
7. Ebrahim SM, Boghdady S, Mohana MA, Rashed M, Th AF, Abbas AM. Integrated GPR analysis and numerical modelling for discovering archaeological mysteries at Kom Ombo temple. *NRIAG J Astron Geophys.* 2024 Dec 31; 13 (1): 106-17. https://doi.org/10.1080/20909977.2024.2372964
8. Pham MT, Lefèvre S. Buried object detection from B-scan ground penetrating radar data using Faster-RCNN [Internet]. arXiv; 2018 [accessed 2025-08-16]. Available from: http://arxiv.org/abs/1803.08414
9. Alexakis E, Lampropoulos K, Doulamis N, Doulamis A, Moropoulou A. DEEP LEARNING APPROACH FOR THE IDENTIFICATION OF STRUCTURAL LAYERS IN HISTORIC MONUMENTS FROM GROUND PENETRATING RADAR IMAGES. 2022 Jan 17 [accessed 2025-08-16]; Available from: https://zenodo.org/record/5772558
10. Mojahid A, Ouai DE, Amraoui KE, El-Hami K, Aitbenamer H. Intelligent recognition of subsurface utilities and voids: A ground penetrating radar dataset for deep learning applications. *Data Brief*. 2025 Apr; 59: 111338. https://doi.org/10.1016/j.dib.2025.111338
11. Frid M, Frid V. A Case Study of the Integration of Ground-Based and Drone-Based Ground-Penetrating Radar (GPR) for an Archaeological Survey in Hulata (Israel): Advancements, Challenges, and Applications. *Appl Sci.* 2024 May 18; 14 (10): 4280. https://doi.org/10.3390/app14104280
12. Green A. Detecting Graves in GPR Data: Assessing the viability of machine learning for the interpretation of graves in B-scan data using medieval Irish case studies. PhD Thesis. 2020;347.
13. Warren C, Giannopoulos A, Giannakis I. gprMax: Open source software to simulate electromagnetic wave

propagation for Ground Penetrating Radar. *Comput Phys Commun*. 2016 Dec; 209: 163-70. https://doi.org/10.1016/j.cpc.2016.08.020
14. Giannopoulos A. Modelling ground penetrating radar by GprMax. *Constr Build Mater*. 2005 Dec; 19 (10): 755-62. https://doi.org/10.1016/j.conbuildmat.2005.06.007
15. Bai X, Yang Y, Wei S, Chen G, et al. A Comprehensive Review of Conventional and Deep Learning Approaches for Ground-Penetrating Radar Detection of Raw Data. *Appl Sci*. 2023 July 7; 13 (13): 7992. https://doi.org/10.3390/app13137992
16. Rao TK, Rajan EG. Ground Penetrating Radar Based Subsurface Imaging of Targeted Buried Objects. 2020; 10 (12).
17. Maharana K, Mondal S, Nemade B. A review: Data pre-processing and data augmentation techniques. *Glob Transit Proc*. 2022 June; 3 (1): 91-9. https://doi.org/10.1016/j.gltp.2022.04.020
18. Vogelsang DC, Erickson BJ. Magician's Corner: 6. TensorFlow and TensorBoard. *Radiol Artif Intell*. 2020 May 1; 2 (3): e200012. https://doi.org/10.1148/ryai.2020200012
19. Romero R, Celard P, Sorribes-Fdez JM, Seara Vieira A, Iglesias EL, Borrajo L. MobyDeep: A lightweight CNN architecture to configure models for text classification. *Knowl-Based Syst*. 2022 Dec; 257: 109914. https://doi.org/10.1016/j.knosys.2022.109914
20. Guo Q, Yang PJ, Wu R, Zhang Y. Numerical Modeling of GPR for Underground Multi-pipes Detection by Combining GprMax and Deep Learning Model. *Prog Electromagn Res M*. 2024; 128: 99-113. https://doi.org/10.2528/PIERM24062603
21. Kullaa J. Sensor validation using minimum mean square error estimation. *Mech Syst Signal Process*. 2010 July; 24 (5): 1444-57. https://doi.org/10.1016/j.ymssp.2009.12.001
22. Ebrahim SM, Boghdady S, Mohana M, Rashed M, Abdel Fattah TA, Abbas AM. FDTD Simulations for Ground Penetrating Radar to Improve Efficiency of Archaeological Investigation [Internet]. SSRN; 2024 [accessed 2025-08-16]. Available from: https://www.ssrn.com/abstract=4698863. https://doi.org/10.2139/ssrn.4698863
23. Bornik A, Neubauer W. 3D Visualization Techniques for Analysis and Archaeological Interpretation of GPR Data. *Remote Sens*. 2022 Apr 1; 14 (7): 1709. https://doi.org/10.3390/rs14071709
24. Ristić A, Govedarica M, Pajewski L, Vrtunski M, Bugarinović Ž. Using Ground Penetrating Radar to Reveal Hidden Archaeology: The Case Study of the Württemberg-Stambol Gate in Belgrade (Serbia). *Sensors*. 2020 Jan 22; 20 (3): 607. https://doi.org/10.3390/s20030607
25. Liu B, Ren Y, Liu H, Xu H, et al. GPRInvNet: Deep Learning-Based Ground-Penetrating Radar Data Inversion for Tunnel Linings. *IEEE Trans Geosci Remote Sens*. 2021 Oct; 59 (10): 8305-25. https://doi.org/10.1109/TGRS.2020.3046454
26. Wang J, Chen H, Lin J, Li X. A Method to Detect Concealed Damage in Concrete Tunnels Using a Radar Feature Vector and Bayesian Analysis of Ground-Penetrating Radar Data. *Buildings*. 2024 Nov 18; 14 (11): 3662. https://doi.org/10.3390/buildings14113662
27. Lei W, Luo J, Hou F, Xu L, Wang R, Jiang X. Underground Cylindrical Objects Detection and Diameter Identification in GPR B-Scans via the CNN-LSTM Framework. *Electronics*. 2020 Oct 31; 9 (11): 1804. https://doi.org/10.3390/electronics9111804
28. Santos CFGD, Papa JP. Avoiding Overfitting: A Survey on Regularization Methods for Convolutional Neural Networks. *ACM Comput Surv*. 2022 Jan 31; 54 (10s): 1-25. https://doi.org/10.1145/3510413
29. Zou L, Li Y, Munisami K, Alani AM. Bridging Theory and Practice: A Review of AI-Driven Techniques for Ground Penetrating Radar Interpretation. *Appl Sci*. 2025 July 23; 15 (15): 8177. https://doi.org/10.3390/app15158177
30. Dai Q, Lee YH, Sun HH, Ow G, Yusof MLM, Yucel AC. DMRF-UNet: A Two-Stage Deep Learning Scheme for GPR Data Inversion Under Heterogeneous Soil Conditions. *IEEE Trans Antennas Propag*. 2022 Aug; 70 (8): 6313-28. https://doi.org/10.1109/TAP.2022.3176386
31. Glocker B, Pauly O, Konukoglu E, Criminisi A. Joint Classification-Regression Forests for Spatially Structured Multi-object Segmentation. Berlin, Heidelberg: Springer Berlin Heidelberg; 2012; p. 870-81. https://doi.org/10.1007/978-3-642-33765-9_62
32. Imai T, Mizutani T, Iguchi T, Haneda T. Enhancing Deep Learning-Based GPR Data Inversion With Unsupervised Domain Adaptation: Comparison of Domain Classifiers. *IEEE Trans Geosci Remote Sens*. 2025; 63: 1-16. https://doi.org/10.1109/TGRS.2025.3568384